# Performance Enhancement of Doubly-Fed Induction Generator-Based-Wind Energy System

Tarek A. Boghdady*‡, Islam A. Sweed*, Doaa Khalil Ibrahim*
* Department of Electrical Power Engineering, Faculty of Engineering, Cairo University, Giza 12613, Egypt
(engtarek82@cu.edu.eg, islamsweed92@gmail.com, doaakhalil73@eng.cu.edu.eg)

‡ Corresponding Author; Tarek A. Boghdady, Tel: +201020443386, engtarek82@cu.edu.eg

*Received: 13.11.2022 Accepted: 26.12.2022*

**Abstract-** Nowadays, the challenging errand is enhancing the wind energy system (WES) performance to be more competitive and economically viable. One of the best ways to enhance the performance of the doubly-fed induction generator (DFIG)-based-WES is the optimization of the proportional-integral (PI) controllers for the variable frequency converter system. Many objectives with different optimization techniques have been used in literature to achieve optimal performance. Each choice has its advantages and disadvantages. This paper presents a new design approach for better performance of PI controllers and, hence DFIG over a wide range of operating conditions through two main themes. The first is by introducing a new multi-objective formulation, while the second is utilizing recent optimization techniques like Grey Wolf Optimizer and Whale Optimization Algorithm. Four PI controllers are optimized using a traditional objective function and the proposed multi-objective formulation. Two are related to the Rotor Side Converter (RSC), named power regulator, and the main rotor side converter current regulator. The other two PI controllers related to Grid Side Converter (GSC) are the DC-link voltage regulator and the main grid-side converter current regulator. A performance comparison is held through normal and abnormal operating conditions on a simulation model of a 6 MW wind farm located in Jabal Alzayt along the Red Sea Coast in Egypt and directly connected to the grid. The results confirmed the effectiveness of the proposed approach to help the DFIG-based-WES to agree with the Egyptian Grid Code during disturbances compared with the traditional objective formulation.

**Keywords** Doubly-Fed Induction Generator (DFIG), Grid Side Converter, Optimization Algorithms, Rotor Side Converter, Wind Energy System (WES).

## 1. Introduction

Recently, wind energy has become an increasingly vital role in electrical power generation all over the world. This type of energy source is developed due to the growing demand for electricity and the trend to use renewable and non-polluting energy sources worldwide [1]. For Egypt, the penetration level of wind farms into the Egyptian electricity grid has increased considerably in the last two decades [2]. The capacity of the existing wind power stations in Egypt now is 1635 MW, shared between Zafrana, Jabal Alzayt, Ras Ghareb, and Gharb Bakr by 33.33%, 35.47%, 15.9%, and 15.3%, respectively [3]. Besides, the integrated and sustainable energy strategy seeks to diversify energy sources and ensure energy reliability. It is worth noting that there are wind farm stations under preparation with a capacity of more than 2800 MW; meanwhile, the total installed capacity of renewable energy sources will reach 19.2 GW by the end of 2022, with 69.27% for wind energy contribution [4].

Jabal Alzayt wind farm is established along the Red Sea Coast on one hundred square kilometers. It is considered one of the largest stations in electricity generation in terms of the number of turbines, capacity, area, and the utilization of new technologies such as the migratory birds monitoring system. This monitoring system is achieved with the help of the radar for stopping the turbines when the migrant birds are passing and restarting them again after confirming that they have passed peacefully [4]. The total capacity of Jabal Alzayt wind farm station is 580 MW, established in three phases. The first phase consists of 120 turbines with a 240 MW capacity, of which only 100 are grid-connected. The second phase comprises 110 turbines with 220 MW capacity, where 75 turbines are linked to the grid with 150 MW capacity. The third phase is 60 turbines with 120 MW capacity [3]. Accordingly, the studied model in this paper will be a part of the network of an air-insulated substation (AIS) in one of the new promising projects in Jabal Alzayt, which utilizes the doubly-fed induction generator based-wind energy system (DFIG-based-WES).

In DFIG, the induction generator (IG) directly connects to the grid through stator terminals. On the other hand, the rotor terminals are grid-connected throughout a variable frequency converter system (VFCS) and coupling transformer. The VFCS manages approximately 25-30% of the total power to achieve generator control. The variable speed wind turbine (VSWT) with DFIG is the best choice over the fixed speed wind turbine coupled with IG and VSWT with a synchronous generator [5]. The VSWT with DFIG can provide tracking for the maximum power point, decoupling control of generator reactive and active powers, besides improving the dynamic

performance during power system disturbances such as short circuits and voltage sags. Furthermore, the VFCS of the VSWT with DFIG is smaller and cheaper than VSWT equipped with a synchronous generator where the stator directly connects to the grid via a full-load VFCS. However, the VFCS and IGBT (insulated-gate bipolar transistor) power electronics converters are the most sensitive and vulnerable part of the DFIG-based-WES, as they are exposed to transient disturbances within the grid. The protection from overcurrent in the rotor circuit may cause the Rotor Side Converter (RSC) of the VFCS to be blocked and stops switching because of disturbances, and the turbine may trip. Thus, the VFCS behavior and the associated WES depend on the performance of the DFIG control system. The chance for the WES to stay in service during the grid disturbances increases with the optimally designed controllers. To control the nonlinear components within the power systems, different contemporary control strategies like intelligent and adaptive approaches have been extensively studied [6]-[7]. Still, these control strategies have few real applications, perhaps because of the difficulty of their online tuning, nonlinearity, and their complex structures [8]. As a result, the conventional PI controllers are still a more common control technique in power systems in controlling DFIG-based-WES because of the simple design as demonstrated in [8-11]. Accordingly, the PI controller will be investigated in this paper to be significantly enhanced.

The nonlinearity and complexity of the system make it difficult to tune the PI gains properly. Several singular objective functions are applied in [9] using the Chaotic Whale Optimization Algorithm (CWOA) and the Particle Swarm Optimization (PSO) to improve the reactive power control capability of DFIG. In addition, ensuring the optimal energy harvesting with the aid of marine predators algorithm in [12] and minimizing the distorted currents in the rotor circuit in [13]. On the other hand, the researchers in [11] have preferred implementing the (PSO) in a multi-objective formulation to minimize the steady state error, and achieve the maximum power point Tracking. The controller performance has also improved in [14] during grid faults. As many objective functions have been chosen in literature to achieve optimal performance via different optimization methods, the authors believe it is possible to achieve the best behavior of the controllers through two main themes. The first theme is to accomplish the best formulation for the desired objective function, while the second theme is to use the best optimization method that leads to the best results, which is extensively studied and implemented in this paper. The results display how the proposed formulation can obtain the optimal PI controller parameters. These parameters will significantly improve the DFIG-based-WES dynamic performance over a wide range of operating circumstances.

The rest of the article is divided into several sections. Section 2 presents the DFIG-based-WES configuration and its control system. It also highlights the VSWT and generator modeling and describes the interaction among systems. The studied system is briefly demonstrated in Section 3, in addition to the gains of PI controllers to be tuned. Accordingly, moving on to Section 4 as the paper core, it will introduce the new proposed formulation. Validation of the new proposed objective function is discussed in Section 5. Finally, the conclusion is summarized in Section 6.

## 2. Doubly-Fed Induction Generator-based-Wind Energy System (DFIG-based-WES)

The DFIG is one of the highest leading technologies used in WES due to its singularity in energy harvesting, better performance, cost, and size [5]. The configuration of DFIG-based-WES, the control system, and VSWT modeling will be briefly overviewed in the following subsections.

### *2.1. Configuration of DFIG-Based-WES*

It mainly consists of a wind turbine, DFIG, VFCS, coupling transformer, and control system, as illustrated in Fig. 1. The stator of DFIG is directly grid-connected, and the rotor side is linked to the grid via a VFCS. The power flow between the circuit of the rotor, and the utility grid must be controlled and monitored in both magnitude and direction to generate electrical power at constant voltage and frequency; to the utility grid over the great operation range from sub-synchronous to super synchronous speed [15]. Consequently, each VFCS includes two four-quadrant IGBTs converters joined back-to-back through the DC-link capacitors.

### *2.2. Control System of DFIG-Based-WES*

As depicted in Fig. 1, there are three different control levels in VSWT [5]. The regulation of the power flow between the DFIG and the grid is targeted by the first control level (I). The Rotor Side Converter Control System (RSCCS) aims to provide independent control of both stator's active and reactive powers. The Grid Side Converter Control System (GSCCS) keeps a constant DC-link voltage regardless of the direction and magnitude of the rotor power [16]-[17]. In addition, this control level has a decisive say in the control strategy of the crowbar. The second level of control (II), named by the Wind Turbine Control Strategy (WTCS), is dedicated to controlling the energy conversion from wind energy into mechanical energy. It also computes the needed references for control level (I). All actions concerning the integration between the WT and the grid are related to the third control level (III), the Wind Turbine Grid Integration Strategy (WTGIS).

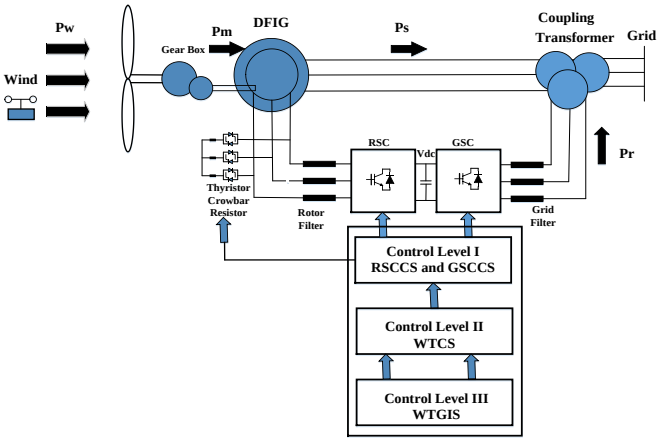


**Fig. 1.** Configuration and control of DFIG-based-WES.

According to [5], a concept called Wind Farm Centralized Control (WFCC) is developed to ensure that the wind farm behaves as one single unit as in conventional power plants. WFCC aims to regulate the injected active and reactive powers at the Point of Common Coupling (PCC).

Due to the wind energy penetration in the Egyptian grid, control of wind farms has become one of the main tasks for Egyptian Grid Operators (EGOs). The Egyptian Grid Code (EGC) has been exploited to set a technical requirement to achieve the main pivotal, that the electricity supplies become in service [16]. Figure 2 clarifies that; the inputs of WFCC will be the references received from EGOs, the measurements from the PCC, and both status and availability of power for each wind turbine (WT) at any time [5]. According to these input data, the WFCC should provide each WT with the references for active and reactive powers. Therefore, it is essential to ensure that there are real-time communications between WFCC, EGOs, and each WT.

### 2.3. VSWT Modeling

This part provides the basic concepts of VSWT and the routine to connect with the grid [5]. It also covers the interaction among systems to formulate the overall VSWT model, as illustrated in Fig. 3.

#### 2.3.1. Aerodynamic System

The aerodynamic system represents the extracted power of the rotor and the turbine torque ($T_t$) according to the angular speed of the turbine ($\omega_t$) and the average wind speed ($V_W$).

#### 2.3.2. Mechanical System

The mechanical depiction of the entire WT is very complex. The mechanism of a WT and the forces experienced by its components are numerous. The mechanical system estimates the angular speed of the turbine and the generator ($\omega_t$, $\omega_m$) depending on their torques ($T_t$, $T_{em}$).

#### 2.3.3. Pitch Control System

The target of the pitch controller is rotating all WT blades at the same angle or each one of them independently. The regulation of independency gives a higher level of freedom to the control system. The pitch system appraises the dynamics of the pitch angle ($\beta$) based on the referenced pitch ($\beta_{ref}$) from the WTCS.

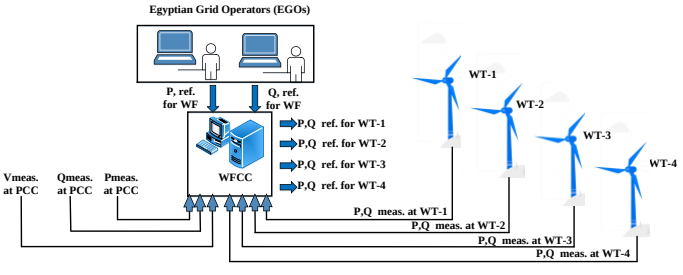


**Fig. 2.** The signals flow among EGOs, WFCC, and WTCS.

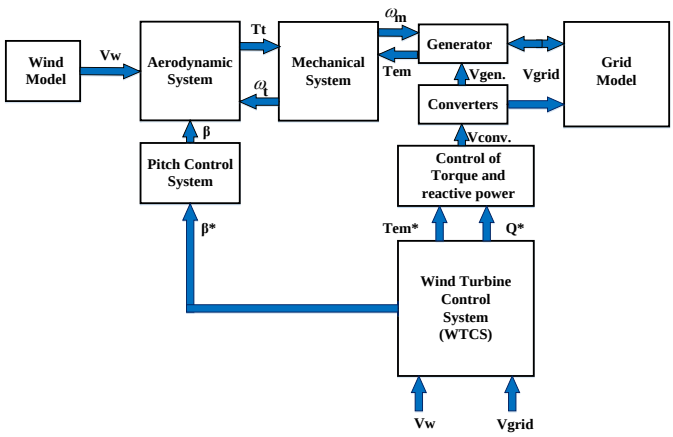


**Fig. 3.** Interaction among VSWT systems.

#### 2.3.4. Electrical System

The main goal of the wind turbine control strategy is to calculate the references of generator torque ($T_{emref}$), reactive power ($Q_{ref}$), and pith angle ($\beta_{ref}$) as a function of grid voltage ($V_{grid}$) and the average wind speed ($V_W$). The conventional aim of the generator is to produce a grid current as a function of the grid voltage ($V_{grid}$).

The DFIG model can be presented in the $dq$ reference frame, and the rotor side quantities are referred to the stator side. The $dq$ voltages equations for the stator ($v_{ds}$,$v_{qs}$) and rotor ($v_{dr}$,$v_{qr}$) are expressed in equations (1-2), while the flux expressions for the stator ($\psi_{ds}$, $\psi_{qs}$) and rotor ($\psi_{dr}$, $\psi_{qr}$) are defined in equations (3-4) [15]:

$$v_{ds} = i_{ds}\, r_s + \frac{d\psi_{ds}}{dt} - \omega\psi_{qs} \;\&\; v_{qs} = i_{qs}\, r_s + \frac{d\psi_{qs}}{dt} - \omega\psi_{ds} \quad (1)$$

$$v_{dr} = i_{dr}\, r_r + \frac{d\psi_{dr}}{dt} - (\omega - \omega_r)\psi_{qr} \;\&\; v_{qr} = i_{qr}\, r_r + \frac{d\psi_{qr}}{dt} + (\omega - \omega_r)\psi_{dr} \quad (2)$$

$$\psi_{ds} = i_{ds}\, L_s + i_{dr}\, L_m \;\&\; \psi_{qs} = i_{qs}\, L_s + i_{qr}\, L_m \quad (3)$$

$$\psi_{dr} = i_{dr}\, L_r + i_{ds}\, L_m \;\&\; \psi_{qr} = i_{qr}\, L_r + i_{qs}\, L_m \quad (4)$$

Where:

- The subscripts $d$, $q$, $s$, and $r$ refer to $d$ axis, $q$ axis, stator, and rotor quantities, respectively.
- The stator and rotor currents in $dq$ frame are denoted by $i_{ds}$, $i_{qs}$, $i_{dr}$, and $i_{qr}$, respectively.
- $r_s, r_r$ are the winding resistances of the stator and rotor, respectively.
- The angular velocities for the reference frame and the DFIG rotor are presented by$\omega$,$\omega_r$ respectively.
- The stator and rotor inductances ($L_s, L_r$) can be defined in terms of mutual inductance ($L_m$), the leakage inductances of the stator and rotor ($L_{ls}, L_{lr}$) by $L_s = L_{ls} + L_m$ and $L_r = L_{lr} + L_m$.

Accordingly, for the generator slip ($S$), the active and reactive powers of the stator ($P_s$, $Q_s$) and rotor ($P_r$, $Q_r$) will be expressed in equations (5-6).

$$P_s = \frac{3}{2}(v_{ds}\, i_{ds} + v_{qs}\, i_{qs}) \;\&\; Q_s = \frac{3}{2}(v_{qs}\, i_{ds} - v_{ds}\, i_{qs}) \quad (5)$$

$$P_r = \frac{3}{2}\left(v_{dr}\, i_{dr} + v_{qr}\, i_{qr}\right) = -S\, P_s \;\&\; Q_r = \frac{3}{2}\left(v_{qr}\, i_{dr} - v_{dr}\, i_{qr}\right) \quad (6)$$

For the pole pair ($p$), the electromagnetic torque ($T_{em}$) is expressed by:

$$T_{em} = \frac{3}{2} p L_m (i_{qs}\, i_{dr} - i_{ds}\, i_{qr}) \quad (7)$$

## 3. Studied System

The configuration studied here, as demonstrated in Fig. 4, is a part of the transformer network of a 6 MW wind farm located in the Jabal Alzayt region. It consists of four similar 1.5 MW wind turbines (with identical gains) coupled with an AIS substation through a 0.69-22 kV transformer to be connected to the grid through two feeders; 22 kV of 10 km, 220 kV of 20 km, and a 22/220 kV transformer.

The simulation parameters of the studied system are mentioned in Table 1. MATLAB/SIMULINK software is utilized to simulate and test this system taking into account the recommendations of the EGC as in Table 2 [16].

### *3.1. Applied Controllers*

Among the different control strategies examined in the literature, the vector control technique with PI controllers is the most common in DFIG-based-WES [18]. Thus it is selected to be applied in this study. The transfer function of the PI controller is generally given by the next equation, where $K_p$ and $K_i$ are the proportional and the integral gains, respectively [19]:

$$G_c(s) = K_p + \frac{K_i}{s} \quad (8)$$

#### *3.1.1. Control Loops of RSC*

The stator flux-oriented vector control (SFOVC) is deployed for the RSCCS [20]. As demonstrated in Fig. 5 (a); the main focus of the RSCCS is to control the stator terminal voltage ($V_s$) via the PI AC voltage regulator, and the active power ($P_s$) via the PI power regulator, through $d$ and $q$ axes loops, respectively [15].

As shown, controlling $P_s$ and $V_s$ in SFOVC mainly depends on $I_{rabc}$ and its transformation to $I_{dr}$ and $I_{qr}$. The error signals are produced by subtracting the actual signals $P_S, V_s,\ I_{dr}$, and $I_{qr}$ from their reference values $P_s^*, V_s^*,\ I_{dr}^*$, and $I_{qr}^*$, respectively. Then, the error signals of the rotor currents $e_{idr}$, and $e_{iqr}$ are multiplexed before entering the last PI of the RSC current regulator. This PI controller generates a $V_{dqr}$, the voltage signal that will be de-multiplexed again to produce $V_{dr}$, and $V_{qr}$ signals. They are connected to a PWM module to create the IGBT gate corresponding signal of RSC. Some references have a set value such as $V_s^*$ equals 1 p.u, and the corresponding PI AC regulator transforms and generates the $d$ component of rotor current reference ($i_{dr}^*$). Others depend on the power-speed tracking characteristic curve as in $P_s^*$ which transforms and generates the $q$ component of rotor current reference ($i_{qr}^*$) through its corresponding PI power regulator.

**Table 1.** Main simulation parameters of the studied system

| System Description | Parameters | | Values |
|---|---|---|---|
| DFIG | Rated power | | 1.5 MW |
| | Rated voltage | | 690 V |
| | Frequency | | 50 Hz |
| | Stator resistance & inductance | | 0.00706 p.u, 0.171 p.u |
| | Rotor resistance &inductance | | 0.005 p.u, 0.156 p.u |
| | Pole pairs | | 2 |
| | Mutual inductance | | 2.9 p.u |
| | Inertia constant | | 5.04 s |
| | Friction factor | | 0.01 p.u |
| Wind Turbine | Rotor diameter | | 77 m |
| | Cut-in wind speed | | 4 m/s |
| | Nominal wind speed | | 14 m/s |
| | Cut-off wind speed | | 25 m/s |
| | Gear ratio | | 104 |
| | Air density | | 1.225 kg/m$^3$ |
| Wind turbine transformer | Rated Power | | 8 MVA |
| | Winding 1 | Voltage | 690 V |
| | | Resistance | 0.0081 p.u |
| | | Inductance | 0.0453 p.u |
| | Winding 2 | Voltage | 22×10$^3$ V |
| | | Resistance | 0.0081 p.u |
| | | Inductance | 0.0453 p.u |
| PCC bus transformer | Rated Power | | 50 MVA |
| | Winding 1 | Voltage | 22×10$^3$ V |
| | | Resistance | 0.0051 p.u |
| | | Inductance | 0.065 p.u |
| | Winding 2 | Voltage | 220×10$^3$ V |
| | | Resistance | 0.0051 p.u |
| | | Inductance | 0.065 p.u |
| TL line | Positive and zero sequences resistance | | 0.1153 Ω/km, 0.413 Ω/km |
| | Positive and zero sequences inductance | | 1.05×10$^{-3}$ H/km, 3.32×10$^{-3}$ H/km |
| | Positive and zero sequences capacitance | | 11.33×10$^{-9}$ F/km, 5.01×10$^{-9}$ F/km |

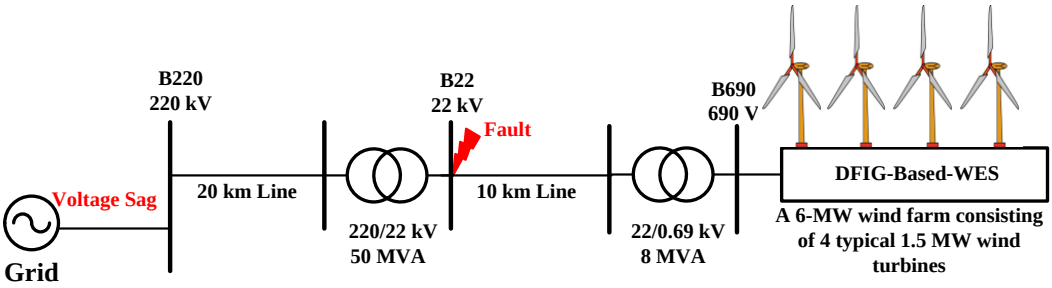


**Fig. 4.** Single line diagram of the studied 6 MW wind farm.

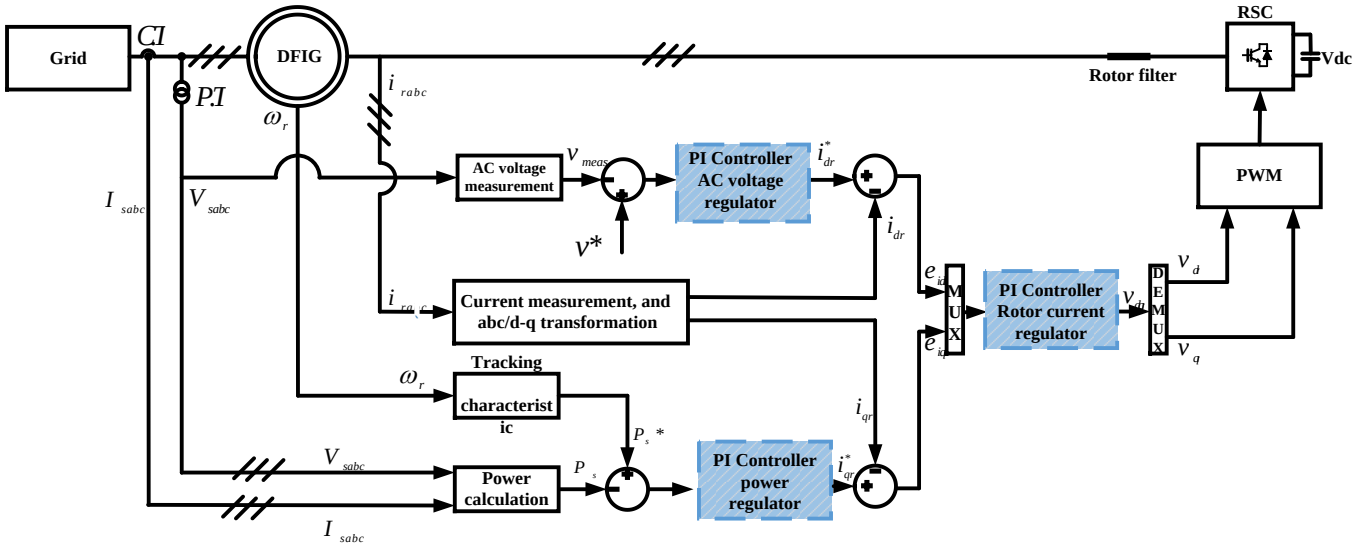


(a) RSCCS

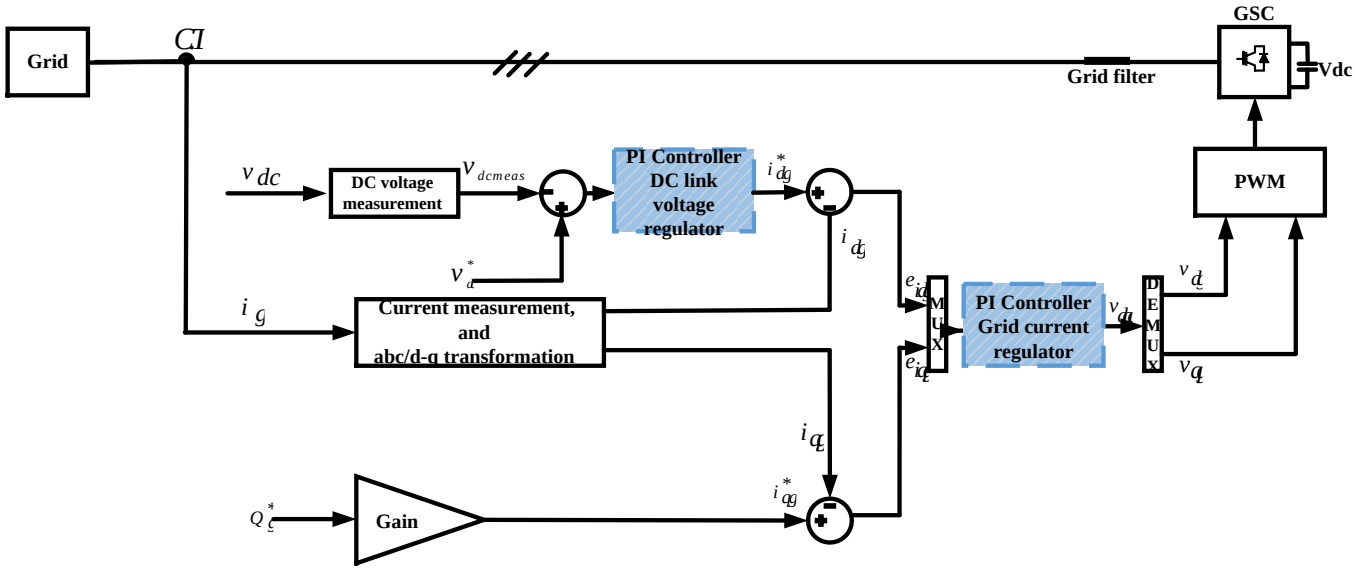


(b) GSCCS

**Fig. 5.** Control loops of (a) RSCCS, (b) GSCCS.

*3.1.2 Control Loops of GSC*

As illustrated in Fig. 5 (b), the GSC is grid-connected at the stator through the grid R-L filter and the DC-link. The main focus of the GSCCS is to ensure that the DC-link voltage is maintained constant [15]. The actual voltage signal ($V_{dc}$) is subtracted from its reference voltage signal ($V_{dc}^*$) which equals 1200 V to generate an error signal, which in turn, becomes an input to the PI controller of the DC-link voltage that provides the reference grid current ($I_{dg}^*$). The reactive power reference ($Q_g^*$) equals zero and the $q$ component of the grid current reference ($i_{qg}^*$) is generated after multiplying with a gain of $\frac{1}{-\frac{3}{2}v_{dg}}$ [17]. A deduction process is implemented between actual signals ($I_{dg}$ and $I_{qg}$) and their references ($I_{dg}^*$ and $I_{qg}^*$)

to form new error signals $e_{idg}$ and $e_{iqg}$, respectively. Then, these errors are multiplexed before going to the PI controller of the GSC current regulator. This PI controller will generate a $V_{dqg}$ voltage signal, which will be demultiplexed again to get finally the two voltage signals $V_{dg}$ and $V_{qg}$. The PWM module will carry out its mission and receive the $V_{dg}$ and $V_{qg}$ signals to create the IGBT corresponding signal of GSC, as revealed in Fig. 5 (b).

### *3.2 PI Controllers Gains*

Once the gains of the PI controllers are correctly tuned, the performance of VFCS is enhanced meaningfully during disturbances. This paper has focused on achieving optimal parameters of PI controllers for both rotor and grid side loops. As demonstrated in Fig. 5, there are five PI controllers for RSCCS and GSCCS for each wind turbine. Three PI controllers are applied for the RSCCS, where the AC voltage and power regulators are combined and multiplexed for the main rotor side converter current regulator. On the other side, there are two PI controllers for the GSCCS, the DC-link voltage regulator and the main grid side converter current regulator. It is worth noting that the gains of the PI AC voltage controller will not be optimized in this study for RSCCS as it is inherently a part of the rotor current PI controller. The gains will be assumed by 1.25 and 300 for the proportional and the integral gain, respectively, as discussed in [20]. Consequently, eight gains of the other four PI controllers need to be optimized for RSCCS and GSCCS for each wind turbine. For simplification, these gains are replicated in the four wind turbines in the studied system. Accordingly, only eight gains will be optimized instead of thirty-two. These gains are power regulator gains ($K_{pp}, K_{ip}$), rotor-side converter current regulator gains ($K_{pr}, K_{ir}$) for RSCCS, DC-link voltage regulator gains ($K_{pv}, K_{iv}$), and grid-side converter current regulator gains ($K_{pg}, K_{ig}$) for GSCCS.

**Table 2.** EGC Recommendations for protection devices

| Functions | EGC Recommended settings | |
|---|---|---|
| | Level | Setting time (s) |
| Under-voltage range < 0.1-1 $U_{nominal}$ | 0.8 $\boldsymbol{U_{nominal}}$ | 3 |
| Under-voltage range << 0.1-1 $U_{nominal}$ | 0.3 $U_{nominal}$ | 0.3-1 |
| Over-voltage range >> 1-1.3 $U_{nominal}$ | 1.2 $U_{nominal}$ | ≤ 3 |
| Over-frequency range > 50-52 Hz | 51.5 Hz | ≤ 0.1 |
| Under-frequency range < 47.5-50 Hz | 47.5 Hz | ≤ 0.5 |

### *3.3 Applied Optimization Algorithms*

Since tuning these PI controllers is wearisome and tedious, different optimization techniques have been employed in this study, such as GA, CSA, Grey Wolf Optimizer (GWO), and Whale Optimization Algorithm (WOA). Mathematical representation and details for the applied optimization algorithms GA, CSA, GWO, and WOA can be found in [21], [22], [23], and [24], respectively. The initial parameters needed to set up optimization algorithms are assigned in Table 3.

## 4. Formulation of Objective Functions

Substantial literature is available for formulating the objectives to tune the PI controllers. Several researchers have applied singular objectives such as [9], [11-13]. Others preferred to specify multiple objectives as in [10], and [14]. Based on different formulations achieved via numerous optimization methods in several reported studies [9], [12], [20], [25], and [26], a satisfactory performance can be obtained by integrating squares of errors. So, the first conception in this paper is to apply this traditional objective function by utilizing different optimization techniques such as CSA and WOA.

### *4.1. Traditional Objective Function (TOF)*

The concept here is to minimize the Integral Square Errors (ISE). Figure 6 illustrates the error cycle that starts by comparing the reference set point and the actual feed-backed measured values to generate the error signal that will be squared and finally integrated to formulate this objective function.

**Table 3.** Initial parameters for optimization algorithms

| | |
|---|---|
| Dimension | 8 [$K_{pv}, K_{iv}, K_{pp}, K_{ip}, K_{pr}, K_{ir}, K_{pg}, K_{ig}$] |
| Max. No. of iterations | 500 |
| Search agents /population | 30 |
| Lower bounds | [0.1, 50, 0.1, 50, 0.1, 0.1, 0.1, 50] |
| Upper bounds | [50, 500, 50, 500, 50, 50, 50, 500] |

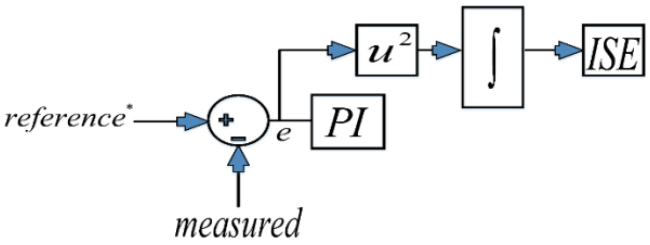


**Fig. 6.** The concept of TOF.

Now, the four studied PI controllers are optimized simultaneously, and thus the traditional objective function is formulated as defined in Eq. (9).

$$Minimize\ ISE = \int_0^{\infty} [w_1 e_p^2 + w_2 e_r^2 + w_3 e_v^2 + w_4 e_g^2](t)\ \ dt \tag{9}$$

Where $e_p$ and $e_r$ are the RSCCS error signals of the stator active power regulator and rotor side converter current regulator, respectively. For GSCCS, $e_v$ and $e_g$ are the error signals of the DC-link voltage regulator and the grid-side converter current regulator, respectively. The weighting factors for the four error values are presented by $w_1, w_2, w_3$, and $w_4$, while their summation must be equal to one. It is worth noting that assigning weighting factors by operators relies on the required priority. For this study, the weighting factors are assumed to be similar and equal $\frac{1}{4}$. The optimized gains using TOF in normal starting conditions are indicated in Table 4. As noticed, the fitness function value of WOA is better than the CSA. The DC-link voltage in normal starting conditions using CSA and WOA is further checked to affirm different indices, such as the settling time and overshoot. Moreover, the performance is also assessed for different fault types, as will be introduced in the following subsections.

### *4.1.1 Examining Optimized PI Controllers Using TOF In Normal Starting Conditions*

The behavior of the DC-link voltage in normal starting conditions with TOF is demonstrated in Fig. 7. When applying CSA and measuring the performance criteria, it was found that the settling period was about 0.72 seconds, while the overshoot and undershoot percentages were 13 and 11%, respectively. It is also checked whether there would be a clear improvement in the controller performance when applying WOA as a more advanced optimization method. It was noticed that there is no remarkable improvement in the settling period by using the optimal parameters based on WOA. In contrast, the overshoot is enhanced from 13% to 10.3%, and the undershoot is also improved from 11% to 9.7%. In conclusion, despite that TOF gives an acceptable performance in normal starting conditions but still needs improvement, especially in settling time.

### *4.1.2 Examining Optimized PI Controllers Using TOF For Different Fault Types*

A single line-to-ground (L-G), two line-to-ground (L-L-G), and three line-to-ground (3L-G) faults are investigated to evaluate the performance of TOF during disturbances through the WOA-based gains. All fault types are simulated on the 22 kV line, as indicated in Fig. 4, to occur at t=15 seconds and last for five cycles. Subsequently, the indices for the corresponding sudden change in active power, capacitive current injection, and DC-link voltage, shown in Fig. 8, are analyzed and indicated in Table 5.

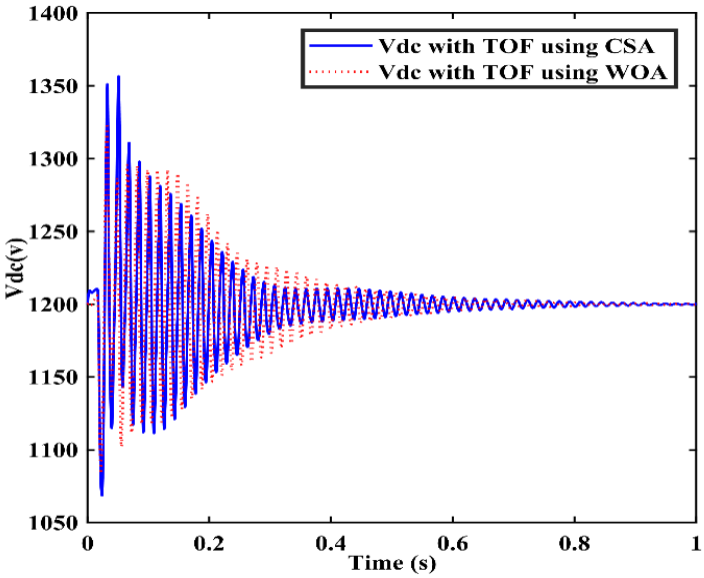


**Fig. 7.** DC-link voltage during normal starting conditions for optimized PI controllers with TOF using CSA and WOA.

**Table 4.** Gains of optimized PI controllers for each turbine using TOF

| Optimization Algorithm | DC-link voltage regulator | | Power regulator | | RSC current regulator | | GSC current regulator | | Value of Fitness Function |
|---|---|---|---|---|---|---|---|---|---|
| | $K_{pv}$ | $K_{iv}$ | $K_{pp}$ | $K_{ip}$ | $K_{pr}$ | $K_{ir}$ | $K_{pg}$ | $K_{ig}$ | |
| CSA | 12 | 500 | 2.8 | 346 | 3.25 | 10.5 | 0.97 | 222 | $8.78\times10^{-14}$ |
| WOA | 7.6 | 469 | 3.4 | 432 | 0.17 | 18.4 | 2.07 | 178.5 | $10.23\times10^{-16}$ |

**Table 5.** Different indices for the performance of optimized PI controllers with TOF using WOA during different fault type

| Performance Criteria | L-G fault | | | L-L-G fault | | | 3L-G fault | | |
|---|---|---|---|---|---|---|---|---|---|
| | $V_{dc}$ (v) | $P$ $(MW)$ | $Q$ $(MVar)$ | $V_{dc}$ (v) | $P$ $(MW)$ | $Q$ $(MVar)$ | $V_{dc}$ (v) | $P$ $(MW)$ | $Q$ $(MVar)$ |
| Settling Time (s) | 0.376 | 0.22 | 0.38 | 0.31 | 0.24 | 0.23 | 0.135 | 0.153 | 0.153 |
| Overshoot (%) | 9.19 | 12.93 | 10.01 | 22.67 | 23.57 | 59.89 | 121.2 | 0 | 10.96 |
| Undershoot (%) | 7.1 | 12.12 | 577.05 | 11.25 | 2.48 | 611.75 | 0 | 100 | 401.45 |
| Steady-state status of WT | WT remains in service | | | WT remains in service | | | WT disconnects | | |

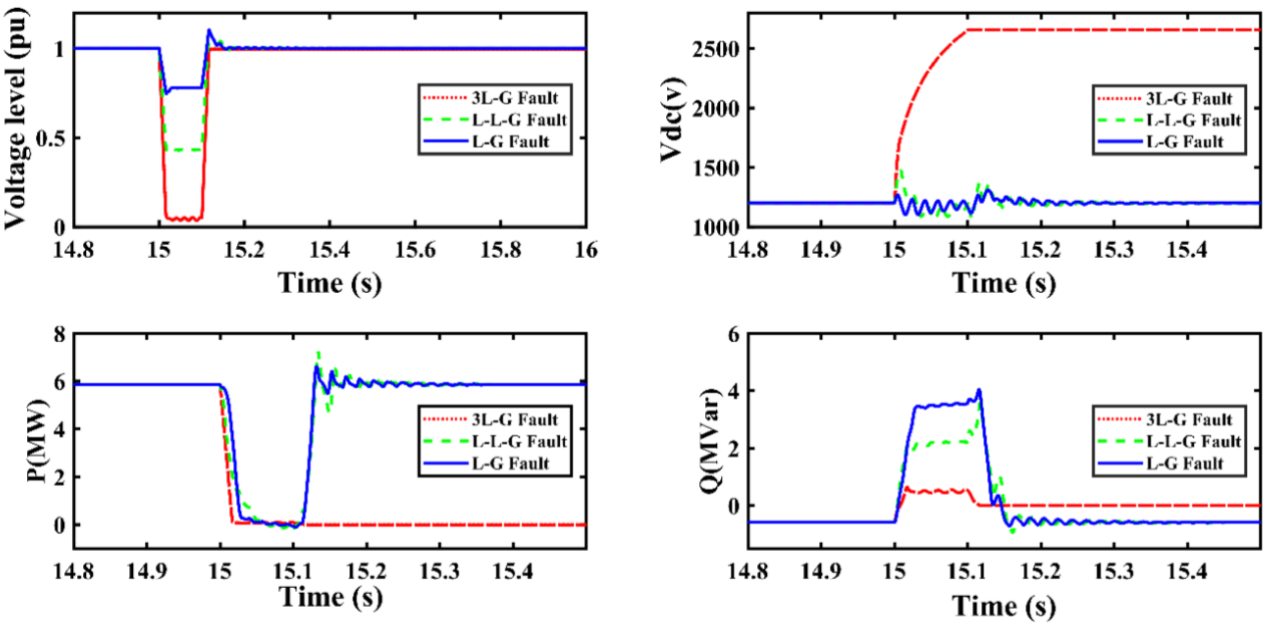


**Fig. 8.** Performance of optimized PI controllers with TOF using WOA for different fault types.

*4.2. The Proposed Formulation of a Multi-Objective Function*

For achieving superior performance for the optimized controllers, a new multi-objective formulation is proposed with three objectives. The objectives are minimizing the rotor current overshooting ($\Delta I_r$), the settling time ($T_{sett.}$), and the integral square errors for the four PI controllers as presented in Eq. (10), where $W_1$, $W_2$, and $W_3$ are the weighting factors for the three objectives.

$$Minimize\ \mathrm{F(x)} = \mathrm{W_1\ \Delta I_r + W_2\ T_{sett.}} + \mathrm{W_3} \int_0^{\infty} \left[\frac{1}{4}\mathrm{e_p^2} + \frac{1}{4}\mathrm{e_r^2} + \frac{1}{4}\mathrm{e_v^2} + \frac{1}{4}\mathrm{e_g^2}\right](t)\ dt \quad (10)$$

For the sake of simplicity, this formulation supposes that there is no prioritization, which means equal weighting factors with the value of ( $\frac{1}{3}$ ). A proper normalization has been considered to ensure consistency and scaling among different terms in the proposed multi-objective formulation. At first, the essential step is to find the optimal parameters of the controller within normal operating conditions through this proposed multi-objective formulation. Different optimization techniques are utilized as GA, CSA, WOA, and GWO.

Table 6 presents the optimized PI controllers gains by several optimization techniques. It is vital to evaluate how the DFIG-based-WES has been affected by these newly obtained gains to check the convenience of the proposed multi-objective formulation. Accordingly, a performance comparison will be deployed in the following subsections between TOF and the new proposed formulation during normal starting conditions and different fault types.

*4.2.1 Performance Comparison Between TOF And The Proposed Formulation In Case Of Normal Starting Conditions*

A performance comparison is applied between TOF and the proposed formulation under the same normal starting conditions. The DC-link voltage is checked here as illustrated in Fig. 9. Once looking, it can be noticed that there is a significant improvement for the proposed formulation, especially in the low ripples and the shortest settling time of only 0.195 seconds instead of 0.72 seconds for the TOF. The overshooting percentage was 13.58 % for the new proposed formulation, 13 %, and 10.3 % for the TOF using CSA and WOA, respectively. Although the preference is still the best fit for the TOF concerning the overshooting percentage improvement, the undershooting is enhanced in the proposed formulation to be only 3.85% instead of 11% and 9.7% for the TOF using CSA and WOA, respectively.

**Table 6.** Gains of optimized PI controllers for each turbine using the proposed multi-objective formulation

| Optimization Algorithms | DC link voltage regulator | | Power regulator | | RSC current regulator | | GSC current regulator | | Value of Fitness Function |
|---|---|---|---|---|---|---|---|---|---|
| | $K_{pv}$ | $K_{iv}$ | $K_{pp}$ | $K_{ip}$ | $K_{pr}$ | $K_{ir}$ | $K_{pg}$ | $K_{ig}$ | |
| GA | 1.87 | 285 | 0.89 | 122.3 | 0.5 | 8.7 | 0.47 | 122 | $2.35\times10^{-8}$ |
| CSA | 6.55 | 310 | 8.6 | 135 | 2.74 | 9.9 | 2.6 | 106.5 | $0.896\times10^{-8}$ |
| GWO | 5 | 372 | 4.2 | 103.1 | 1.6 | 12.3 | 1 | 94 | $1.4\times10^{-10}$ |
| WOA | 1.34 | 306 | 1.9 | 105 | 0.3 | 9 | 8.7 | 100 | $0.747\times10^{-10}$ |

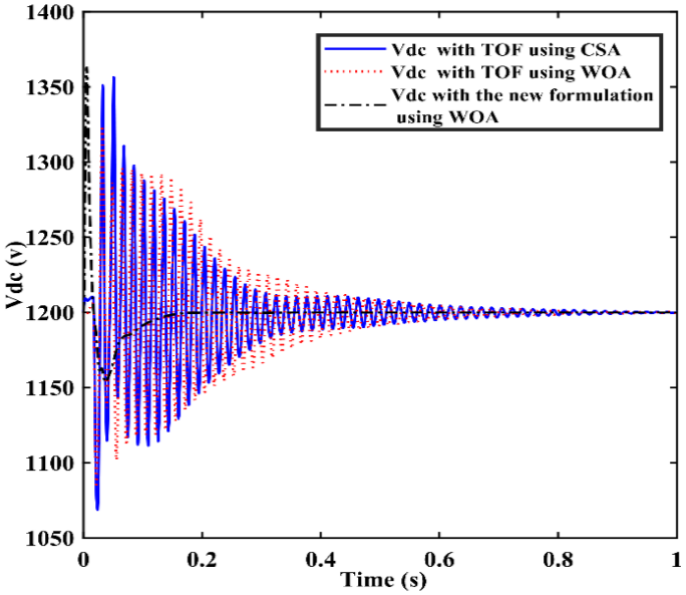


Fig. 9. DC-link voltage during normal starting conditions for optimized PI controllers using the proposed multi-objective formulation compared with TOF.

*4.2.2 Performance Comparison Between TOF And The Proposed Formulation In Case Of Different Fault Types*

Figure 10 depicts the optimized controllers' performance using the proposed multi-objective formulation during fault conditions. The three fault types (L-G, L-L-G, and 3L-G) are simulated at the same conditions described in section 4.1.2. In addition, the results in Tables 7, 8, and 9 summarize the effect of the proposed multi-objective formulation on the DC-link voltage, active power, and reactive power for L-G, L-L-G, and 3L-G faults, respectively.

Over these tabulated results in Tables 7, 8, and 9, it is clarified that implementing the proposed formulation using CSA provides better performance for DC-link voltage through less overshooting, less undershooting, and less settling time in case of L-G fault. Also, the WOA, GA, and GWO are the best algorithms for active power regarding settling time, overshooting, and undershooting. On the other hand, the TOF using WOA gives good results regarding reactive power overshooting, whereas the proposed formulation with WOA still provides better settling times.

Considering the L-L-G faults, the results in Table 8 assure that the GWO and WOA offer superior performance than the other optimization algorithms. Unfortunately, the proposed formulation using GA or CSA does not give the expected results, as the turbine becomes out of service, similar to the case of TOF using WOA. Nevertheless, the WOA acquires the preference in the case of 3L-G fault, as shown in Table 9, through lower overshooting in DC-link voltage (89.48 %) while the system withstands successfully. Although GWO provides good dynamic behavior during faults, there is still an overshooting with a value of 102.11 % for the DC-link voltage.

## 5. Compatibility with Egyptian Grid Code (EGC)

In this study, the PI controller gains are designed at the rated speed of 14 m/s with normal operating conditions. However, the system's dynamic performance during disturbances should agree with the EGC. So, the general requirements according to EGC will be presented at the beginning of this section. Then, the system's dynamic behavior is extensively evaluated during several disturbances [27], such as permanent faults, grid voltage sag, and wind speed variation.

### *5.1 General Requirements of EGC*

The general requirements of EGC can be summarized in the following [16]:

- Regarding the voltage and the frequency operating ranges, the EGC specifies that the grid-connected wind farm operates continuously and delivers available active power according to the wind conditions whenever the frequency range of 47.5-51.5 Hz and the voltage range of 0.85-1.1 p.u of the nominal voltage at PCC. Also, EGC specifies the period requirements and regions of the wind farm's output power during different variations of frequency and voltage at PCC.
- The EGC obliges the WF to operate at the nominal active power at PCC within the range of 0.95 lagging - 0.95 leading power factor.
- The reactive power capability (RPC) is only required when the active power is equal to or higher than 20 % of the rated power. The RPC must decrease linearly for the lower values of the active power.
- For the low voltage ride-through (LVRT) and the dynamical regulations during and after faults, Fig. 11 (a) demonstrates the profile of the Egyptian LVRT curve for grid-connected wind farms. The EGC necessitates that WFs remain in service when the grid voltage is at zero volts for a period that does not exceed 7.5 cycles.
- During faults, the EGC requests a capacitive current injection to improve the voltage at PCC as displayed in Fig. 11 (b).
- After faults, the EGC imposes other technical requirements for the active power restoration rate. For example, the active power of the generator must be restored to the pre-fault power within ten seconds after the fault clearance. Also, the absorption of the reactive power shall equal the consumption value before the fault or less.
- The grid-connected wind farm should have the ability to become in service and deliver its power in normal operating conditions unless there is a malfunction in any of EGC requirements, for example:
  - Instantaneous overcurrent: 10 p.u.
  - Maximum current ($I_1$): 1.1 p.u for 5 s.
  - Maximum current unbalance ($I_2/I_1$ p.u): 0.4 for 0.2 s.
  - Under-voltage and over-voltage ($V_1$): as per the Egyptian LVRT curve in Fig. 11 (a).
  - Under frequency, and over frequency (f): As per indicated in Table 2.
  - Max voltage unbalance for negative, and zero sequences ($V_2/ V_1$), ($V_0/ V_1$) p.u: 0.05 for 0.2 s.

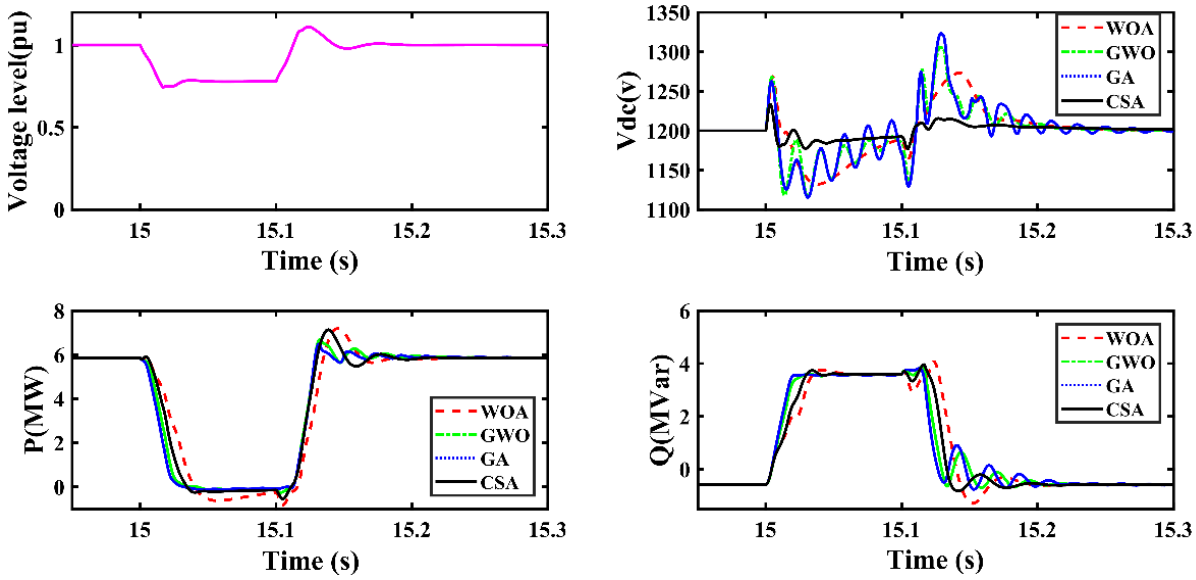


(a) L-G fault

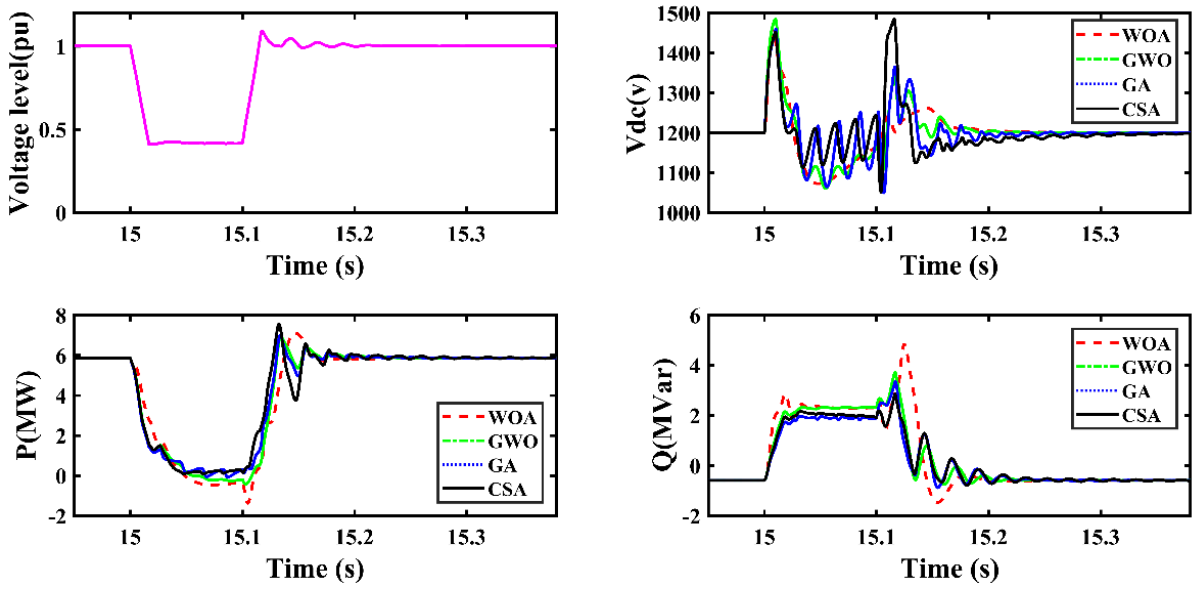


(b) L-L-G fault

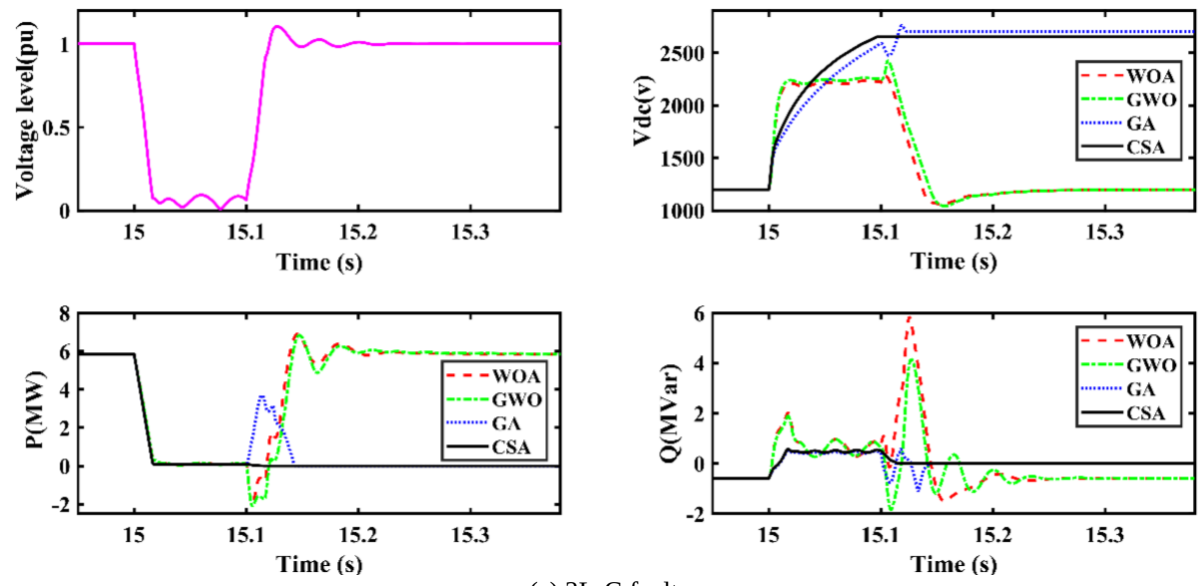


(c) 3L-G fault

**Fig. 10.** Performance of optimized PI controllers using the proposed multi-objective formulation for different fault types.

**Table 7.** Comparing the proposed multi-objective formulation and TOF during L-G fault

| Performance criteria | $V_{dc}$(v) | | | | |
|---|---|---|---|---|---|
| | Proposed multi-objective formulation | | | | TOF using WOA |
| | GA | CSA | GWO | WOA | |
| Settling Time (s) | 0.289 | 0.175 | 0.24 | 0.258 | 0.376 |
| Overshoot (%) | 10.278 | 2.79 | 8.861 | 6.135 | 9.19 |
| Undershoot (%) | 7.06 | 1.93 | 7 | 5.67 | 7.1 |
| Steady-state status of WT | WT remains in service | | | | |
| | | | | | |
| Performance criteria | $P(MW)$ | | | | |
| | Proposed multi-objective formulation | | | | TOF using WOA |
| | GA | CSA | GWO | WOA | |
| Settling Time (s) | 0.31 | 0.22 | 0.19 | 0.18 | 0.22 |
| Overshoot (%) | 10.88 | 21.89 | 14.17 | 22.79 | 12.93 |
| Undershoot (%) | 2.22 | 9.31 | 4.35 | 14.06 | 12.12 |
| Steady-state status of WT | WT remains in service | | | | |
| | | | | | |
| Performance criteria | $Q(MVar)$ | | | | |
| | Proposed multi-objective formulation | | | | TOF using WOA |
| | GA | CSA | GWO | WOA | |
| Settling Time (s) | 0.21 | 0.23 | 0.20 | 0.19 | 0.38 |
| Overshoot (%) | 29.74 | 40.56 | 19.365 | 120.06 | 10.01 |
| Undershoot (%) | 650.938 | 675.87 | 664.189 | 699.838 | 577.05 |
| Steady-state status of WT | WT remains in service | | | | |

**Table 8.** Comparing the proposed multi-objective formulation and TOF during L-L-G fault

| Performance criteria | $V_{dc}$(v) | | | | |
|---|---|---|---|---|---|
| | Proposed multi-objective formulation | | | | TOF using WOA |
| | GA | CSA | GWO | WOA | |
| Settling Time (s) | 0.263 | 0.328 | 0.19 | 0.205 | 0.31 |
| Overshoot (%) | 21.68 | 23.78 | 23.739 | 21.619 | 22.67 |
| Undershoot (%) | 12.52 | 12.33 | 11.55 | 10.59 | 11.25 |
| Steady-state status of WT | WT remains in service | | | | |
| | | | | | |
| Performance criteria | $P(MW)$ | | | | |
| | Proposed multi-objective formulation | | | | TOF using WOA |
| | GA | CSA | GWO | WOA | |
| Settling Time (s) | 0.19 | 0.24 | 0.188 | 0.1632 | 0.24 |
| Overshoot (%) | 19.78 | 29.07 | 18.66 | 21.59 | 23.57 |
| Undershoot (%) | 1.40 | 6.05 | 4.78 | 23.44 | 2.48 |
| Steady-state status of WT | WT remains in service | | | | |
| | | | | | |
| Performance criteria | $Q(MVar)$ | | | | |
| | Proposed multi-objective formulation | | | | TOF using WOA |
| | GA | CSA | GWO | WOA | |
| Settling Time (s) | 0.22 | 0.27 | 0.20 | 0.19 | 0.23 |
| Overshoot (%) | 49.87 | 33.97 | 26.427 | 152.241 | 59.89 |
| Undershoot (%) | 570.81 | 490.43 | 634.201 | 827.97 | 611.75 |
| Steady-state status of WT | WT remains in service | | | | |

**Table 9.** Comparing the proposed multi-objective formulation and TOF during 3L-G fault

| Performance criteria | $V_{dc}$(v) | | | | |
|---|---|---|---|---|---|
| | Proposed multi-objective formulation | | | | TOF using WOA |
| | GA | CSA | GWO | WOA | |
| Settling Time (s) | 0.12 | 0.1 | 0.236 | 0.221 | 0.135 |
| Overshoot (%) | 129.97 | 120.94 | 102.11 | 89.48 | 121.2 |
| Undershoot (%) | 0 | 0 | 13.14 | 11.48 | 0 |
| Steady-state status of WT | WT disconnects | WT disconnects | WT is still in service | WT is still in service | WT disconnects |
| | | | | | |
| Performance criteria | $P(MW)$ | | | | |
| | Proposed multi-objective formulation | | | | TOF using WOA |
| | GA | CSA | GWO | WOA | |
| Settling Time (s) | 0.14 | 0.115 | 0.25 | 0.23 | 0.153 |
| Overshoot (%) | 0 | 0 | 16.7 | 18 | 0 |
| Undershoot (%) | 100 | 100 | 135.6 | 134.55 | 100 |
| Steady-state status of WT | WT disconnects | WT disconnects | WT is still in service | WT is still in service | WT disconnects |
| | | | | | |
| Performance criteria | $Q(MVar)$ | | | | |
| | Proposed multi-objective formulation | | | | TOF using WOA |
| | GA | CSA | GWO | WOA | |
| Settling Time (s) | 0.14 | 0.12 | 0.25 | 0.25 | 0.153 |
| Overshoot (%) | 92.34 | 0 | 213.5 | 155.5 | 10.96 |
| Undershoot (%) | 97.75 | 99.8 | 709.14 | 992.41 | 401.45 |
| Steady-state status of WT | WT disconnects | WT disconnects | WT is still in service | WT is still in service | WT disconnects |
| | | | | | |

It is worth highlighting that different points A, B, C, D, E, and F, demonstrated in Fig. 11, are the tested cases discussed in Section 5.2.

*5.2. Testing the Performance for Permanents Faults*

Several permanent faults are also examined to ascertain whether the system performance and behavior are consistent and comply with the EGC or not. The evaluated cases are four cases for permanent faults simulated to occur at t=15 seconds, as shown in Table 10.

For 1st and 2nd tested fault cases, Fig. 12 indicates that the wind turbine is still in service in these cases. It matches with the coordinates of A and B points in the "No trip region" illustrated in Fig. 11 (a). In contrast with the 3rd and 4th tested fault cases, Fig. 13 ensures that the wind turbine will disconnect for both cases due to either the lower voltage dip value with a higher duration or the higher voltage dip value with a lower interval. The performance agrees with the LVRT curve in Fig. 11 (a) as the points C and D are in the "Trip region".

Figure 11 (b) illustrates the trials to enhance the voltage level by injecting a capacitive reactive current. It has the value of E (1 p.u equals 3.59 MVar) for the case of fault points A and C and has the value of F (approximately 0.67 p.u equals 2.34 MVar) in the case of B and D. By these tests, the system has proven its ability to overcome the permanent faults per the EGC requirements and its good dynamic behavior to adopt and restore during the abnormal conditions.

**Table 10.** Tested cases for permanent faults

| C/Cs / Fault Case | Voltage Dip Value (p.u) | Voltage Dip Duration (s) | Case's coordinates according to LVRT in Fig. 11 (a) | Turbine Status |
|---|---|---|---|---|
| 1st Case | 0.781 | 1.5 | A | WT remains in service |
| 2nd Case | 0.437 | 0.5 | B | WT remains in service |
| 3rd Case | 0.781 | 3 | C | WT disconnects |
| 4th Case | 0.431 | 2.5 | D | WT disconnects |

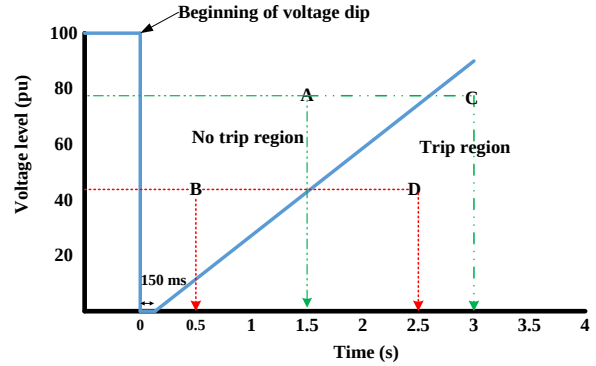


(a) LVRT Profile

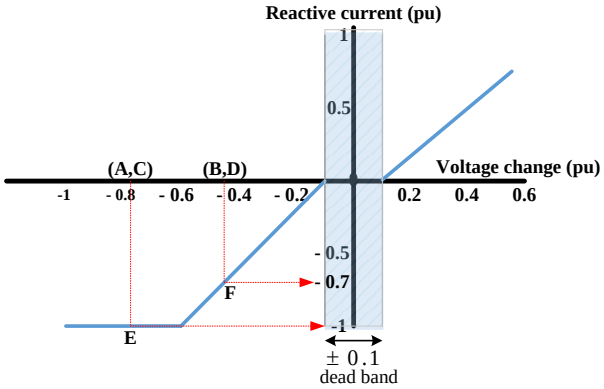


(b) Dynamical regulation during disturbances

**Fig. 11.** LVRT and dynamical regulations according to EGC.

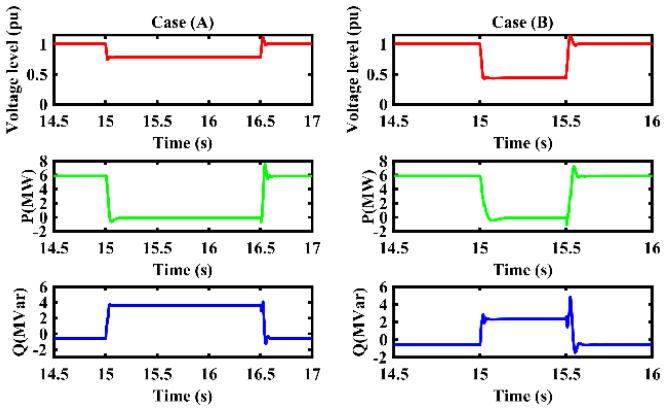


**Fig. 12.** Per unit voltage, $P(MW)$, and $Q(MVar)$ for fault cases A and B.

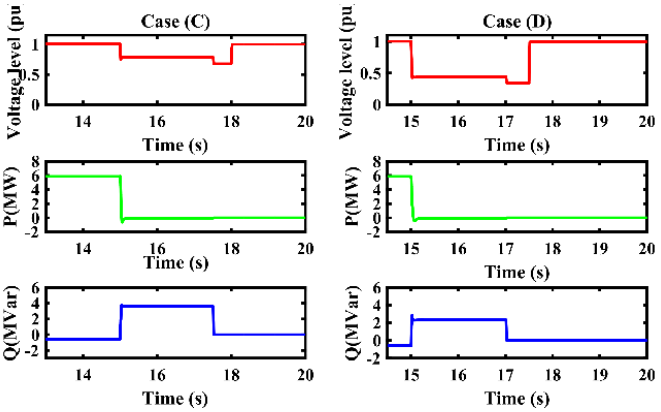


**Fig. 13.** Per unit voltage, $P(MW)$, and $Q(MVar)$ for fault cases C and D.

*5.3. Grid Voltage Sag*

Voltage sag is one of the most common disturbances in the utility grid [28]-[29]. The system is further evaluated under this sudden drop in voltage to ensure rapid restoration to its normal conditions. An instantaneous voltage sag occurs on the 220 kV system. It has a value of 0.5 p.u and occurs at t=15 seconds for 0.5 seconds. The simulated sag in the grid voltage causes the voltage level at the wind turbine bus to be 0.64 p.u, as shown in Figure 14 (a). Figure 14 (b) proves that the system behavior can quickly return to its stable mode.

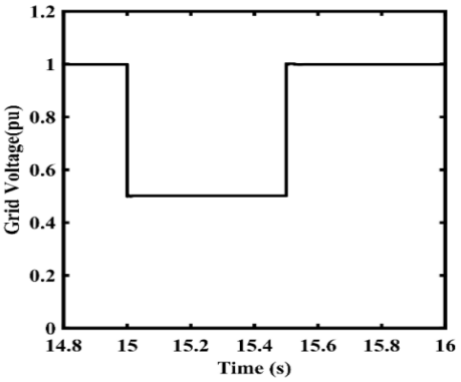


(a) Grid voltage profile

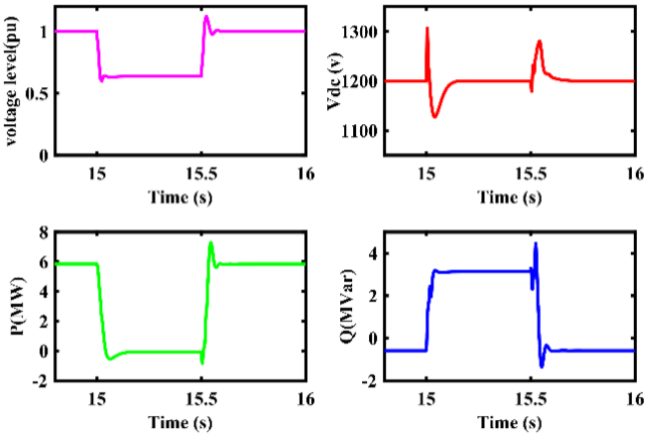


(b) Per unit voltage, DC-link voltage (V), $P(MW)$, and $Q(MVar)$

**Fig. 14.** Performance of optimized PI controllers with proposed multi-objective formulation using WOA in case of a grid voltage sag.

*5.4. Testing the Performance for Wind Speed Variation*

According to IEC Standard 61400-1 [30], the wind speed ($V_w$) profile demonstrated in Fig. 15 will witness different variations within 300 seconds. The wind speed is assumed to be 8 m/s for sixty seconds, then increases gradually to 14 m/s in sixty seconds, after that remains constant at the rated speed of 14 m/s for sixty seconds, and then gradually reduces in sixty seconds to remain fixed for the last sixty seconds at the value of 10 m/s. Figure 15 presents the system's dynamic response toward such simulated wind speed variation. As shown, the active power is directly proportional to the cube of wind speed. So, at the rated speed, the wind farm produces approximately its rated output power of 6 MW. The DC-link voltage is not noticeably affected as its value is only changed by plus or minus 0.16% during the wind speed variation.

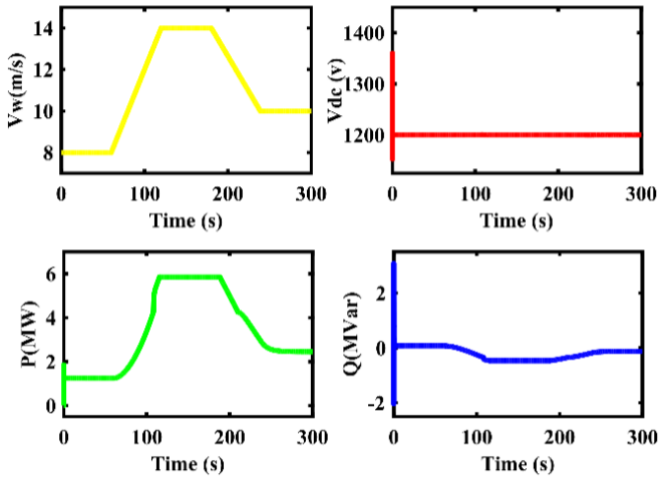


**Fig. 15.** $V_w(m/s)$, $V_{dc}(V)$, $P(MW)$, and $Q(MVar)$ in case of wind speed variation.

*5.5.Testing The Performance When Using Several Combinations Of Weighting Factors In Normal Starting Conditions.*

As discussed before, assigning weighting factors by operators relies on the required priority. In this section, several combinations of weighting factors ($W_1, W_2,$ and $W_3$) are investigated by evaluating the performance of the optimized PI controllers using the proposed multi-objective formulation. Therefore, three tested cases are carried out by different weighting factors to generate the new optimized gains demonstrated in Table 11 through 300 iterations of WOA.

From Fig. 16, the performance criteria tend towards giving preference to the second case as it has the least settling time of 0.05 s which is in line with the desired goal as the settling time has 60% priority in the objective function.

## 6. Conclusion

The control system of DFIG-based-WES aims to provide independent control on both stator's active and reactive powers and to keep the DC-link voltage constant. Thus, the properly designed PI controllers for achieving these aims should be identified. In fact, the traditional formulation via only minimizing the integral square errors ensured an acceptable performance during normal operating conditions but still needs significant improvement during disturbances. So, it was the motivation toward developing a formulation to enhance the overall performance during different operating conditions and keep the WES in service through disturbances. A new formulation of a multi-objective function has been proposed to minimize settling time, integral square errors, and overshooting percentage. The normalization process has been considered supposing equal and variable weighting factors. The controllers' parameters have been elicited through several recent optimization techniques such as GA, CSA, GWO, and WOA using MATLAB/ SIMULINK software.

Validation and verification studies for the system's dynamic behavior and compatibility with Egyptian Grid code have been done by examining the system during various operating conditions, such as wind speed variations, several fault types, and voltage sags. It is impressive that the attained results from the proposed multi-objective formulation confirm better performance than the traditional formulation, especially during sharp disturbances such as 3L-G faults. The accomplished results are encouraging as the system could adapt and return quickly to its stability mode after each disturbance.

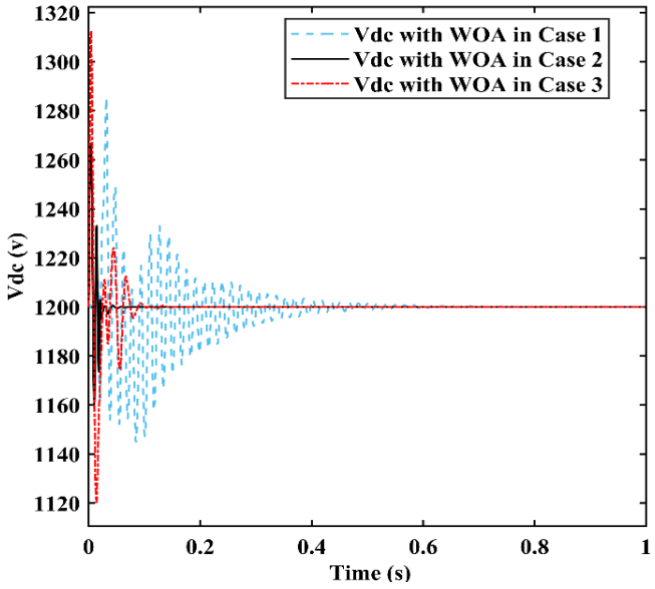


**Fig. 16.** DC-link voltage during normal starting conditions using the proposed multi-objective formulation with different weighting factors

**Table 11.** Gains of optimized PI controllers for each turbine using the proposed multi-objective formulation with different weighting factors by utilizing WOA

| Case #: Weighting Factors | DC link voltage regulator | | Power regulator | | RSC current regulator | | GSC current regulator | | Value of Fitness Function |
|---|---|---|---|---|---|---|---|---|---|
| | $K_{pv}$ | $K_{iv}$ | $K_{pp}$ | $K_{ip}$ | $K_{pr}$ | $K_{ir}$ | $K_{pg}$ | $K_{ig}$ | |
| Case 1: $W_1$=0.2, $W_2$=0.2 and $W_3$=0.6 | 0.29 | 87.8 | 0.42 | 335 | 1.32 | 0.3 | 0.3 | 445 | 0.09962 |
| Case 2: $W_1$=0.2, $W_2$=0.6 and $W_3$=0.2 | 27.8 | 363.3 | 0.15 | 500 | 50 | 0.1 | 0.13 | 131.2 | 0.0075 |
| Case 3: $W_1$=0.6, $W_2$=0.2 and $W_3$=0.2 | 43.4 | 451.17 | 0.1 | 50 | 9.95 | 11.77 | 0.41 | 281.15 | 0.0045 |

## References

[1] O. Alkul, D. Syed and S. Demirbas, "Review of Wind Energy Conversion Systems," *10th International Conference on Smart Grid (icSmartGrid)*, Istanbul, Turkey, pp. 72-77, 27-29 June 2022.

[2] M. H. Alham, M. Elshahed, D. K. Ibrahim, and E. Abo El Zahab, "Optimal operation of power system incorporating wind energy with demand side management," *Ain Shams Engineering Journal*, vol. 8, no. 1, pp. 1-7, 2017.

[3] NREA, "nrea.gov.eg," 2022,[Online], last accessed October 2022. Available:http://nrea.gov.eg/test/en/Media/Reports/2021.

[4] IRENA, "irena.org," 2018.[Online], last accessed October 2022 Available:https://www.irena.org/publications/2018/oct/renewable-energy-outlook-egypt.

[5] G. Abad, J. Lopez, M. Rodriguez, L. Marroyo, and G. Iwanski, "Doubly fed induction machine: modeling and control for wind energy generation," John Wiley & Sons, Hoboken, New Jersey, 2011.

[6] H. Benbouhenni, "Utilization of an ANFIS-STSM algorithm to minimize total harmonic distortion", *International Journal of Smart Grid*," vol. 4, no. 2, pp. 56-67, 2020.

[7] N. Ullah, I. Sami, M. S. Chowdhury, K. Techato and H. I. Alkhammash, "Artificial Intelligence Integrated Fractional Order Control of Doubly Fed Induction Generator-Based Wind Energy System," *IEEE Access*, vol. 9, pp. 5734-5748, 2021.

[8] S. Salah, M. S. Chabani, M. Becherif, M. T. Benchouia, H. S. Ramadan, A. Betka, A. Golea, and S. E. Zouzou, "Experimental behaviour analysis for optimally controlled standalone DFIG system," *IET Electric Power Applications*, vol. 13, no. 14, pp. 1462-1473, 2019.

[9] A. D. Falehi, "An optimal second-order sliding mode based inter-area oscillation suppressor using chaotic whale optimization algorithm for doubly fed induction generator," *International Journal of Numerical Modelling*, vol. 35, no. 2, 2022.

[10] M. Ernesto, B. Aguilar, D. V. Coury, R. Reginatto, and R. M. Monaro, "Multi-objective PSO applied to PI control of DFIG wind turbine under electrical fault conditions," *Electric Power Systems Research*, vol. 180, no. 106081, 2020.

[11] B. Hamid, I. Hussain, S. J. Iqbal, B. Singh, S. Das, and N. Kumar, "Optimal MPPT and BES Control for Grid-Tied DFIG-Based Wind Energy Conversion System," *IEEE Transactions on Industry Applications*, vol. 58, no. 6, pp. 7966-7977, 2022.

[12] R. G. Mohamed, M. A. Ebrahim, Z. M. Alaas and M. M. R. Ahmed, "Optimal Energy Harvesting of Large-Scale Wind Farm Using Marine Predators Algorithm," *IEEE Access*, vol. 10, pp. 24995-25004, 2022.

[13] A. Benamor, M. T. Benchouia, K. Srairi, and M. E. H. Benbouzid, "A new rooted tree optimization algorithm for indirect power control of wind turbine based on a doubly-fed induction generator," *ISA Transactions*, vol. 88, pp. 296-306, 2019.

[14] E. Chetouani, Y. Errami, A. Obbadi, and S. Sahnoun, "Optimal tuning of PI controllers using adaptive particle swarm optimization for doubly-fed induction generator connected to the grid during a voltage dip," *Bulletin of Electrical Engineering and Informatics*, vol. 10, no. 5, pp. 2367-2376, 2021.

[15] H. Abu-Rub, M. Malinowski, and K. Al-Haddad, "Power electronics for renewable energy systems, transportation, and industrial applications," Wiley-IEEE Press, West Sussex, United Kingdom, 2014.

[16] S. HE. Abdel Aleem, A. Y. Abdelaziz, and A. F. Zobaa, "Handbook of Distributed Generation," Springer International Publishing AG 2017, pp. 227-245.

[17] G. e. Abad, "Power electronics and electric drives for traction applications," John Wiley& Sons, West Sussex, United Kingdom, 2017.

[18] M. K. Döşoğlu, "Hybrid control approach for low-voltage ride-through capability in doubly-fed induction generator-based wind turbines," *Computers & Electrical Engineering*, vol. 90, no. 106972, 2021.

[19] H. Benbouhenni, and H. Gasmi, "Comparative Study of Synergetic Controller with Super Twisting Algorithm for Rotor Side Inverter of DFIG", *International Journal of Smart Grid*," vol. 6, no. 4, 2022.

[20] S. Salah, H. S. Ramadan, and M. Becherif, "Dynamic behavior analysis for optimally tuned on-grid DFIG systems," *Energy Procedia*, vol. 162, pp. 339-348, 2019.

[21] O. Kramer, "Genetic Algorithm Essentials Studies in Computational Intelligence," Springer, Warsaw, Poland, vol. 679, 2017.

[22] A. G. Hussien, M. Amin, M. Wang, G. Liang, A. Alsanad, A. Gumaei, and H. Chen, "Crow Search Algorithm: Theory, Recent Advances, and Applications," *IEEE Access*, vol. 8, pp. 173548-173565, 2020.

[23] S. Mirjalili, S. M. Mirjalili, and A. Lewis, "Grey wolf optimizer," *Advances in Engineering Software*, vol. 69, pp. 46-61, 2014.

[24] S. Mirjalili, and A. Lewis, "The whale optimization algorithm," *Advances in Engineering Software*, vol. 95, pp. 51 -67, 2016.

[25] O. P. Bharti, R. K. Saket, and S. K. Nagar, "Controller design for doubly fed induction generator using particle swarm optimization technique," *Renewable Energy*, vol. 114, Part B, pp. 1394-1406, 2019.

[26] H. K. R. Alluri , A. S. Tummala, PV. Ramanarao , and M. Krishna, "Optimal Tuning of PI Controllers for DFIG-Based Wind Energy System using Self-adaptive Differential Evolution Algorithm," *International Journal on Electrical Engineering and Informatics*, vol. 11, no. 2, pp. 352-372, 2019.

[27] R. A. Jerin, Amalorpavaraj, P. Kaliannan, U. Subramaniam, and M. S. El Moursi, "Review on FRT solutions for improving transient stability in DFIG-WTs," *IET Renewable Power Generation*, vol. 12, no. 15, pp. 1786-1799, 2018.

[28] R. G. Srinivasa, B. Srikanth Goud, and Ch. Rami Reddy, "Power Quality Improvement using ASO Technique," *9th International Conference on Smart Grid (icSmartGrid*), "Setubal, Portugal, pp. 238-242, 29 June-1 July 2021.

[29] Y. Han, Y. Feng, P. Yang, L. Xu, Y. Xu, and F. Blaabjerg, "Cause, classification of voltage sag, and voltage sag emulators and applications: a comprehensive overview," *IEEE Access*, vol. 8, pp. 1922-1934, 2019

[30] IEC 61400-1:2019, "Wind energy generation systems - Part 1: Design requirements," 2019. [Online].last accessed October 2022 Available https://webstore.iec.ch/publication/64648.